

Modulation Design for Wireless Information and Power Transfer with Nonlinear Energy Harvester Modeling

Ekaterina Bayguzina and Bruno Clerckx

Department of Electrical and Electronic Engineering, Imperial College London, London, U.K.

Email: {ekaterina.bayguzina08, b.clerckx}@imperial.ac.uk

Abstract—Far-field wireless power transfer (WPT) and simultaneous wireless information and power transfer (SWIPT) have become increasingly important in radio frequency (RF) and communication communities recently. The problem of modulation design for SWIPT has however been scarcely addressed. In this paper, a modulation scheme based on asymmetric phase-shift keying (PSK) is considered, which improves the SWIPT rate-energy tradeoff region significantly. The nonlinear rectifier model, which accurately models the energy harvester, is adopted for evaluating the output direct current (DC) power at the receiver. The harvested DC power is maximized under an average power constraint at the transmitter and a constraint on the rate of information transmitted via a multi-carrier signal over a flat fading channel. As a consequence of the rectifier nonlinearity, this work highlights that asymmetric PSK modulation provides benefits over conventional symmetric PSK modulation in SWIPT and opens the door to systematic modulation design tailored for SWIPT.

Index Terms—SWIPT, nonlinear model, rectenna, energy harvesting, modulation.

I. INTRODUCTION

Radio frequency (RF) wireless power transfer (WPT) has become more important recently with the advent of mainly battery free wireless sensor networks and Internet of Things. At the same time, new wireless communications systems enabling simultaneous wireless information and power transfer (SWIPT) are widely investigated in the research community.

With regard to practical modulation schemes, their effect on the energy conversion efficiency (ECE) as compared to continuous wave (CW) transmission has been considered by the RF community [1]-[4]. In [1], FSK modulated signals are shown to be detrimental in terms of harvested power due to the mixing operation of the diode-based rectifier. In [2], amplitude and phase variations introduced by QPSK and 16QAM are demonstrated to decrease the ECE as compared to the CW. However, it is established in [3] that these modulation schemes can improve the ECE at low input powers. In [4], it is shown that the ECE, achieved via multitone and modulated signals, depends on the circuit optimization, mainly on the matching network and the load. Accordingly, such signals can enhance the ECE for certain load values and input power levels in relation to a CW signal with the same average power.

However, modulation schemes designed specifically for the purpose of SWIPT have scarcely been addressed [5].

Moreover, most of the existing works in the SWIPT literature are based on the linear model of the energy harvester (EH) [5]-[9]. Yet, the linear EH model is limited in terms of accuracy, and systematic waveform design utilizing the nonlinear model allows to achieve a higher ECE (and overall end-to-end power transfer efficiency) in a practical rectenna circuit with the use of multiple sinewaves [10]-[13]. Leveraging [10], SWIPT signal design accounting for the rectifier nonlinearity was studied in [14]. It was concluded in [14] that the rectifier nonlinearity radically changes the design of SWIPT. Indeed “it favours a different waveform, modulation, input distribution and transceiver architecture as well as a different use of the RF spectrum. Exploiting the rectifier nonlinearity in the SWIPT design also makes a more efficient use of the resources by enabling enlarged rate-energy regions compared to those obtained by ignoring the nonlinearity in the system design.” Motivated by those observations, the optimal input distribution of SWIPT subject to nonlinear power constraints was studied in [15]-[16]. Remarkably, it was shown that the capacity of an additive white Gaussian noise (AWGN) channel under transmit average power and nonlinear delivered power constraints is the same as the capacity of an AWGN channel under an average power constraint. In other words, the capacity of an AWGN channel is independent of the value of the delivered power constraint. The capacity can be arbitrarily approached by using time sharing between distributions with high amount of information, e.g. circularly symmetric complex Gaussian (CSCG) inputs, and distributions with high amount of power reminiscent of flash signaling exhibiting a low probability of high amplitude signals.

In this paper, motivated by the above observations, we design modulation for SWIPT with nonlinear energy harvester based on finite constellations. We study modulation of information symbols onto the multi-carrier energy-carrying waveform, resulting in a unified SWIPT waveform. We adapt PSK modulation to SWIPT requirements and propose asymmetric PSK modulation, which allows to gain the maximum output energy while maintaining the required information rate.

Notation: $\mathcal{E}\{\cdot\}$ refers to the DC component of a signal. $\mathbb{E}\{\cdot\}$ refers to the expectation over statistical randomness. $\text{Var}\{\cdot\}$ refers to the variance of a random variable. $U[-a, a]$ denotes the uniform distribution over the interval $[-a, a]$. The convolution operator is denoted by $*$.

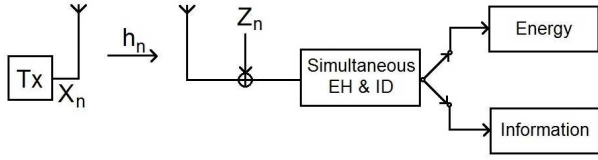


Fig. 1: System model with the receiver simultaneously decoding information and harvesting energy.

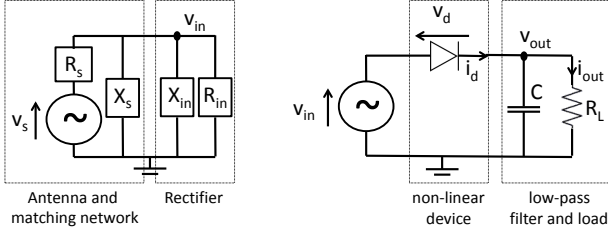


Fig. 2: Antenna equivalent circuit (left) and a single series diode rectifier (right).

II. SWIPT SYSTEM MODEL

We study the system model illustrated in Fig. 1, in which a single-input single-output (SISO) point-to-point SWIPT is considered and the receiver is assumed to be able to simultaneously decode information and harvest energy. We consider a multi-carrier/band transmission (with single-carrier being a special case) consisting of N orthogonal subbands where the n th subband has carrier frequency f_n and equal bandwidth B_s , $n = 0, \dots, N - 1$. The carrier frequencies are evenly spaced such that $f_n = f_0 + n\Delta_f$ with Δ_f denoting the inter-carrier frequency spacing (with $B_s \leq \Delta_f$). The channel, over which the signal is transmitted, is assumed to be flat fading and is subject to AWGN. Throughout the paper, we assume that the effect of noise is negligible for energy harvesting purposes.

A. Transceiver Design

Considering the multi-carrier transmission, the channel input at time t is given as

$$x(t) = \Re \left\{ \sum_{n=0}^{N-1} X_n e^{j2\pi f_n t} \right\} \quad (1)$$

with $X_n = S_n e^{j\Phi_n}$, where S_n and Φ_n refer to the amplitude and phase of the n th carrier at frequency f_n . The transmitter is subject to a transmit power constraint $\mathbb{E}\{|X_n|^2\} \leq P$.

The transmitted signal $x(t)$ propagates through a multipath channel. The received signal at the receiver is modelled as

$$y(t) = \Re \left\{ \sum_{n=0}^{N-1} h_n X_n e^{j2\pi f_n t} \right\}, \quad (2)$$

where h_n is the channel frequency response at frequency f_n .

B. Antenna Equivalent Circuit Model

The antenna model reflects the power transfer from the antenna to the rectifier through the matching network. As

illustrated in Fig. 2 (left), a lossless antenna can be modelled as a voltage source $v_s(t)$ followed by a series resistance R_s and a parallel reactance X_s . The rectifier is modelled as a resistance R_{in} in parallel with a reactance X_{in} . Assuming perfect matching ($R_{in} = R_s$, $X_{in} = -X_s$), all the available RF power $P_{in,av}$ is transferred to the rectifier and absorbed by R_{in} , so that $P_{in,av} = \mathbb{E}\{\mathcal{E}\{|v_{in}(t)|^2\}\}/R_s$. Since $P_{in,av} = \mathbb{E}\{\mathcal{E}\{|y(t)|^2\}\}$, $v_{in}(t) = y(t)\sqrt{R_s}$.

C. Rectifier and Diode Nonlinear Model

Consider a rectifier composed of a single series diode followed by a low-pass filter with a load as in Fig. 2 (right). Denote the voltage drop across the diode as $v_d(t) = v_{in}(t) - v_{out}(t)$ where $v_{in}(t)$ is the input voltage to the diode and $v_{out}(t)$ is the output voltage across the load resistor. A tractable behavioural diode model is obtained by Taylor series expansion of the diode characteristic equation $i_d(t) = i_s(e^{\frac{v_d(t)}{n v_t}} - 1)$ (with i_s the reverse bias saturation current, v_t the thermal voltage, and n the diode ideality factor) around a quiescent operating point $v_d = a$, namely $i_d(t) = \sum_{i=0}^{\infty} k_i (v_d(t) - a)^i$, where $k_0 = i_s(e^{\frac{a}{n v_t}} - 1)$ and $k_i = i_s \frac{e^{\frac{a}{n v_t}}}{i!(n v_t)^i}$, $i = 1, \dots, \infty$. Assume a steady-state response and an ideal low pass filter, such that $v_{out}(t)$ is at a constant DC level. Choosing $a = \mathbb{E}\{\mathcal{E}\{v_d(t)\}\} = -v_{out}$, we can write $i_d(t) = \sum_{i=0}^{\infty} k_i v_{in}(t)^i = \sum_{i=0}^{\infty} k_i R_s^{i/2} y(t)^i$. Truncating the expansion to order 4, the DC component of $i_d(t)$ is obtained as $i_{out} \approx k_0 + z_{DC}$ where

$$z_{DC} = k_2 R_s \mathbb{E}\{\mathcal{E}\{y(t)^2\}\} + k_4 R_s^2 \mathbb{E}\{\mathcal{E}\{y(t)^4\}\} \quad (3)$$

with $k_2 = 0.0034$ and $k_4 = 0.3829$ for a typical Schottky diode with $i_s = 5\mu A$ and $n = 1.05$, and $v_t = 25.86mV$. The reader is referred to [10],[14] for more details on this EH model.

III. MODULATION DESIGN FOR SWIPT

Considering a flat fading channel with gains given as $h_n = 1$ for $n = 1, \dots, N$, we first study the scaling of the harvested power at the receiver with respect to the number of carriers, as well as the variation in the phase range of the transmitted signal. Next, we consider the *MPSK* modulation design for SWIPT purposes and study the achievable information rate for the considered *MPSK* modulation. Finally, we consider optimization of the harvested power under an average power constraint and a received information rate constraint.

A. Scaling Law for Uniformly Distributed Random Phase

An analytical expression for z_{DC} in (3) is now derived for the multi-carrier signal with uniform power allocation across the carriers with $S_n = s = \sqrt{2P/N}$, $n = 0, \dots, N - 1$ and the phases of different carrier frequencies chosen to be independent identically distributed (i.i.d.) as $\Phi_n \sim U[-\delta, \delta]$, $n = 0, \dots, N - 1$. For a flat fading channel, the received signal $y(t)$ is given by

$$y(t) = \sqrt{\frac{2P}{N}} \sum_{n=0}^{N-1} \cos(2\pi f_n t + \Phi_n). \quad (4)$$

The second and fourth order terms in z_{DC} in (3) are simplified by taking the time average and expectation over the randomness of the signal, resulting in

$$z_{DC} = k_2 R_s P + \frac{3k_4 R_s^2 P^2}{2N^2} \sum_{\substack{n_0, n_1, n_2, n_3 \\ n_0 + n_1 = n_2 + n_3}} \mathbb{E}\{\cos(\Theta)\}, \quad (5)$$

where Θ denotes the random term in (5) given by

$$\Theta = \Phi_{n_0} + \Phi_{n_1} - \Phi_{n_2} - \Phi_{n_3}. \quad (6)$$

The resultant probability density function (p.d.f.) of Θ is obtained by convolving four uniform distributions $\Phi_{n_i} \sim U[-\delta, \delta]$, $i = 0, \dots, 3$. The exact distribution of Θ can also be approximated with a normal distribution. In [17], it is shown that the sum of I i.i.d. and uniformly distributed random variables converges to the normal distribution extremely fast. Accordingly, we approximate the distribution of Θ in (6) by a normal distribution $\mathcal{N}(\sum_{i=0}^3 \mathbb{E}\{\Phi_{n_i}\}, \sum_{i=0}^3 \text{Var}\{\Phi_{n_i}\})$ with $\mathbb{E}\{\Phi_{n_i}\} = 0$ and $\text{Var}\{\Phi_{n_i}\} = \frac{\delta^2}{3}$.

Next, the expected mean of the random variable $\cos(\Theta)$ is obtained as $\mathbb{E}\{\cos(\Theta)\} = \Re\{\mathbb{E}\{e^{j\Theta}\}\} = e^{-2\delta^2/3}$.

Finally, noting that there are $N(2N^2 + 1)/3$ terms in the sum of (5), the scaling law for z_{DC} for the signal $y(t)$ in (4) is obtained as

$$z_{DC}(\delta) \simeq k_2 R_s P + k_4 R_s^2 \frac{(2N^2 + 1)}{2N} P^2 e^{-\frac{2\delta^2}{3}}. \quad (7)$$

It is observed that the harvested power given by the z_{DC} metric increases with N but decreases with δ . The rate of scaling of z_{DC} with N is diminished with enlarging the phase range, until it becomes nearly flat for $\Phi_n \sim U[-\pi, \pi]$. Moreover, the case of $\delta = 0$ is equivalent to the scaling exhibited by the deterministic multisine signal in a frequency-flat channel in [10], whereas the case of $\delta = \pi$ leads to a scaling behaviour similar to the multi-carrier signal modulated with CSCG inputs in [14]. Thus, departing from the in-phase condition for maximum power transfer makes it possible to simultaneously transfer information with a phase-modulated multi-carrier signal.

B. Asymmetric MPSK Modulation Design for SWIPT

The scaling law for z_{DC} (7) motivates the use of modulation schemes, in which the symbols are distributed in the limited phase range. Accordingly, this allows to obtain higher gains in harvested power.

Motivated by the WPT observations in Section III.A, for asymmetric MPSK modulation, the symbols are given as $X_n \in \{x_m = se^{\pm j(2m+1)\delta/(M-1)}, m = 0, 1, \dots, \frac{M}{2} - 1 : \delta < \pi\}$, $n = 0, \dots, N - 1$. Note that choosing $\delta = \pi$ yields the standard symmetric MPSK modulation $X_n \in \{x_m = se^{\pm j(m+1)\pi/M}, m = 0, 1, \dots, \frac{M}{2} - 1\}$, $n = 0, \dots, N - 1$. As an example, an asymmetric 4PSK constellation with $\delta = \pi/3$ is illustrated in Fig. 3, along with the decision regions for maximum a posteriori (MAP) decoding at the receiver side.

The resultant probability mass function (p.m.f.) of Θ in (6) is found by discrete convolution of the p.m.f.s of Φ_{n_i} . The

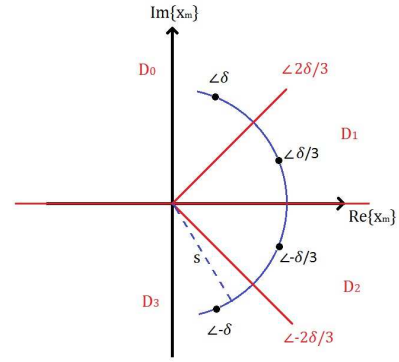


Fig. 3: Asymmetric 4PSK constellation with $\delta = \pi/3$. MAP decision boundaries are shown by red lines.

support of the random variable Θ is the set of values $\{\theta_k = -4\delta + \frac{2\delta k}{M-1}, k = 0, 1, \dots, 4(M-1) : \delta < \pi\}$ for the case of asymmetric MPSK and $\{\theta_k = \frac{(-4(M-1)+k)\pi}{M}, k = 0, 1, \dots, 4(M-1)\}$ for the case of symmetric MPSK.

To account for the discrete distribution of the phases Φ_{n_i} , the scaling law in (7) is modified as follows:

$$z_{DC}(\xi) = k_2 R_s P + k_4 R_s^2 \frac{(2N^2 + 1)}{2N} P^2 \xi, \quad (8)$$

where $\xi = \sum_{k=0}^{4M-4} \cos(\theta_k) \text{Pr}(\Theta = \theta_k)$. Note that the harvested energy is maximized when $\xi = 1$.

For convenience, in (8) we can further write $\xi = \cos(\boldsymbol{\theta}) \bar{\mathbf{p}}^T$, where $\cos(\boldsymbol{\theta}) = [\cos(\theta_0) \dots \cos(\theta_{4M-4})]$ and $\bar{\mathbf{p}} = [\text{Pr}(\Theta = \theta_0) \dots \text{Pr}(\Theta = \theta_{4M-4})]$ are the support of the random variable Θ and the corresponding probabilities obtained as $\bar{\mathbf{p}} = \mathbf{p} * \mathbf{p} * \hat{\mathbf{p}} * \hat{\mathbf{p}}$, respectively. In the latter, $\mathbf{p} = [p_0 \dots p_{M-1}]$ denotes the p.m.f. of the symbols in MPSK constellation using the notation $p_m = \text{Pr}(X = x_m)$ and $\hat{\mathbf{p}} = [p_{M-1} \dots p_0]$ is the reversed version of the vector \mathbf{p} . The reversion is necessary to account for the subtractions of the two random variables Φ_{n_i} in the expression for Θ in (6).

C. Achievable Information Rate

Consider a multi-carrier transmission with N carriers over a flat fading deterministic channel. We aim at maximizing the mutual information $I(\mathbf{X}; \mathbf{Y})$ between the input vector $\mathbf{X} = [X_0 \dots X_{N-1}]$ and the output vector $\mathbf{Y} = [Y_0 \dots Y_{N-1}]$, when the transmitter utilizes asymmetric MPSK modulation with $s = \sqrt{\gamma}$, where γ denotes the signal-to-noise ratio (SNR). We assume that different carriers (subchannels) are statistically independent of each other, i.e. $\text{Pr}(\mathbf{Y}|\mathbf{X}) = \prod_{n=0}^{N-1} \text{Pr}(Y_n|X_n)$. Under this assumption and due to the fact that X_n , $n = 0, \dots, N - 1$ are i.i.d., the achievable rate at the receiver is given by

$$I_N \triangleq I(\mathbf{X}; \mathbf{Y}) = NI(X_0; Y_0). \quad (9)$$

Accordingly, in the following, we equivalently focus on maximizing $I(X_0; Y_0)$. For clarity, we omit the subchannel index. The channel input and output are related through $Y = X + Z$, where Z is an AWGN with standard CSCG distribution $\mathcal{CN}(0, 1)$. The capacity of this channel is obtained by maximizing the mutual information $I(X; Y) = H(Y) - \log_2(\pi e)$.

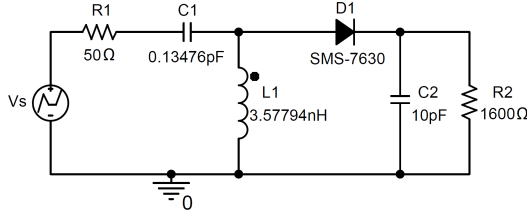


Fig. 4: Rectenna with a single series diode rectifier.

The output entropy $H(Y) = -\int \log_2(p_Y(y))p_Y(y)dy$ is computed by using Monte-Carlo or numerical integration [18], where the output p.d.f. $p_Y(y)$ is given as $p_Y(y) = \sum_{m=0}^{M-1} p_X(x_m)p_Z(y-x_m) = \frac{1}{\pi} \sum_{m=0}^{M-1} p_m e^{-|y-\sqrt{\gamma}e^{j\phi_m}|^2}$.

D. Rate-Energy Region Optimization

We can now define the achievable rate-energy (or, more accurately, rate-DC current) region as $C_{R-IDC}(p_X(x_m)) \triangleq \{(R, I_{DC}) : R \leq I_N, I_{DC} \leq z_{DC}, \sum_{m=0}^{M-1} p_m = 1\}$.

In order to identify the rate-energy region, we formulate the optimization problem as an energy maximization problem subject to rate constraint over the p.m.f. of input symbols:

$$\max_{\{p_m\}} z_{DC} \quad (10)$$

$$\text{subject to } I_N \geq R, \quad (11)$$

$$\sum_{m=0}^{M-1} p_m = 1, \quad (12)$$

where z_{DC} and I_N are given in (8) and (9), respectively.

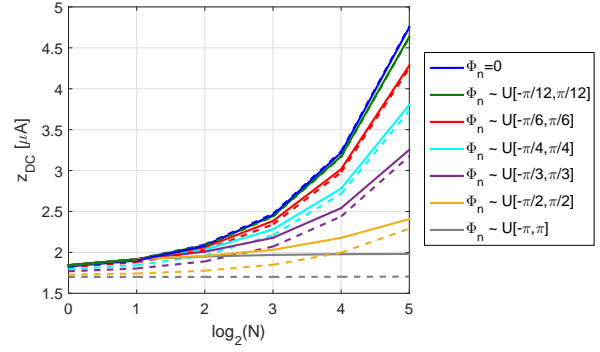
The rate constraint is convex, however, the objective function is non-convex, as it is in essence a signomial function in the variables $\{p_m\}$ as some coefficients $\cos(\theta_k)$ of the products of powers of $\{p_m\}$ are negative in ξ in (8). Since the rate constraint cannot be represented as a posynomial or a signomial, the optimization problem (10)-(12) is not compatible with standard Signomial Geometric Programming (SGP) tools [19]. A locally optimal solution can still be obtained efficiently in MATLAB with Sequential Quadratic Programming (SQP) algorithm [20] that is a quasi-Newton method for solving inequality-constrained nonlinear programming problems.

IV. SIMULATION RESULTS

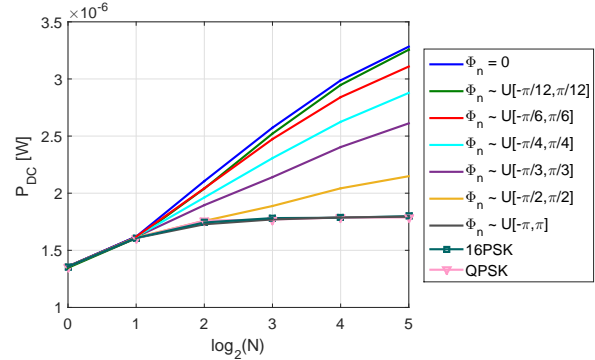
We first present analytical and numerical results for harvested energy with multi-carrier transmission and uniformly distributed random phases. We then show optimization results for the rate-energy region with MPSK modulation. All observations are confirmed by PSpice simulations of a practical rectenna circuit. The rectenna (Fig. 4) is optimized for the input signal composed of 4 in-phase carriers centered around 5.18GHz and the input power level of -20dBm .

A. Results for Random Uniformly Distributed Carrier Phases

Fig. 5a represents z_{DC} as a function of the number of carriers N with the phase of each carrier chosen to be i.i.d. distributed as $\Phi_n \sim U[-\delta, \delta]$. The value of z_{DC} is obtained



(a) z_{DC} obtained numerically (solid lines) and with scaling law (dash lines) as a function of $\log_2(N)$.

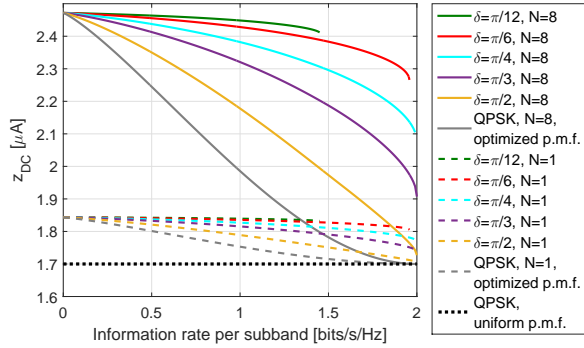


(b) Average DC power P_{DC} as a function of $\log_2(N)$.

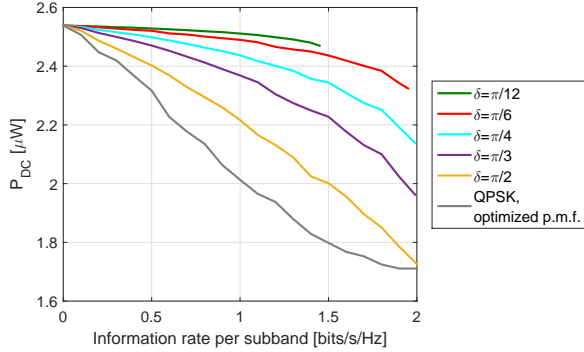
Fig. 5: Results for i.i.d. uniformly distributed carrier phases.

numerically by averaging over several hundred symbol periods using (3). The power P is set as -20dBm and N carriers are centered around 5.18GHz with a frequency gap $\Delta_f = B/N$ for $B = 10\text{MHz}$. The symbol period is set as $T = 1/\Delta_f$. Fig. 5a also illustrates the scaling law in (7) for z_{DC} as a function of the number of carriers N for different values of δ . Apart from the small N region and $\delta = \pi$, there is a good match between the analytical and the numerical results. The inaccuracy between the two is due to the fact that when the carriers with the same index $i = j$ (and, consequently, phase $\Phi_{n_i} = \Phi_{n_j}$) are combined, they contribute constructively to the channel output – this effect is not captured by the analytical approximation in (7).

To validate the scaling laws of Fig. 5a, the rectenna circuit of Fig. 4 is simulated by using the input data signals with uniformly distributed random phase. The PSpice simulations results in terms of the DC output power (Fig. 5b) confirm the analytical and numerical results (Fig. 5a). The P_{DC} behaviour naturally has a more saturated form due to the non-optimality of the circuit design for large N (because of the choice of the finite output capacitor and load). In addition, it is noted that QPSK and 16PSK modulations with equiprobable signaling perform equivalently to the case of $\Phi_n \sim U[-\pi, \pi]$. The harvested DC power is indeed very sensitive to randomness in phase, with the losses due to phase variations increasing with N .



(a) Analytical $C_{R-I_{DC}}$ as a function of δ for $N = \{1, 8\}$ and $M = 4$.



(b) $R - P_{DC}$ region as a function of δ for $N = 8$ and $M = 4$.

Fig. 6: Results for rate-energy region with MPSK modulation.

B. Rate-Energy Region with MPSK Modulation

Fig. 6a illustrates the achievable rate-energy region for 4PSK in various phase range limits for a single ($N = 1$) and multiple ($N = 8$) carrier transmission and SNR of 20dB. The total information rate I_N is normalized w.r.t. the bandwidth NB_s . Hence, the x-axis refers to a per-subband rate. Transmitting over multiple carriers results in higher ECEs – this benefit is added onto the gains due to optimization of the symbols’ p.m.f. relative to the non-optimized equiprobable QPSK, which provides a lower bound for harvested energy. It is also noted that it is possible to significantly enlarge the rate-energy region by limiting the phase range of symbols. Smaller phase ranges $\delta = \{\pi/12, \pi/6\}$ maximize the energy metric most but do not allow to achieve the maximum normalized rate of 2 bits/s/Hz. It can also be derived analytically that for all values of δ , $\xi = 1$ when only one symbol is transmitted with probability 1 giving maximum z_{DC} of $2.47\mu A$ for $N = 8$.

In order to validate those results, the rectenna circuit of Fig. 4 is fed with the input data signals generated for $N = 8$, with the p.m.f. of 4PSK symbols optimized for a set of δ values and at a given rate requirement. The rate- P_{DC} region graph (Fig. 6b) confirms the analytical (Fig. 6a) rate- z_{DC} region results. This validates the EH model and modulation design and highlights the importance of using optimized modulation design in order to increase the ECE of a practical rectenna circuit in the SWIPT configuration.

V. CONCLUSION

In this paper, we optimized the probabilities of symbols for the symmetric and the proposed asymmetric PSK modulations, thereby enlarging the SWIPT rate-energy region considerably as compared to the equiprobable symmetric PSK. Such modulation design is enabled by nonlinear modeling of the EH at the receiver. The gain in harvested energy due to using optimized modulation design is additive to the increase in the ECE achieved by utilizing multiple carriers.

REFERENCES

- [1] H. Sakaki, S. Yoshida, K. Nishikawa, and S. Kawasaki, “Analysis of rectifier operation with FSK modulated input signal,” in *Proc. IEEE Wireless Power Transfer Conf.*, 2013, pp. 187–190.
- [2] H. Sakaki, T. Kuwahara, S. Yoshida, S. Kawasaki, and K. Nishikawa, “Analysis of Rectifier RF-DC Power Conversion Behavior with QPSK and 16QAM Input Signals with WiCoPT System,” in *Proc. Asia-Pacific Microw. Conf.*, 2014, pp. 603–605.
- [3] H. Sakaki, K. Nishikawa, S. Yoshida, and S. Kawasaki, “Modulated scheme and input power impact on rectifier RF-DC Efficiency for WiCoPT system,” in *Proc. 45th Eur. Microw. Conf.*, 2015, pp. 60–63.
- [4] F. Bolos, J. Blanco, A. Collado, and A. Georgiadis, “RF energy harvesting from multi-tone and digitally modulated signals,” *IEEE Trans. Microw. Theory Techn.*, vol. 64, no. 6, pp. 1918–1927, Jun. 2016.
- [5] I. M. Kim and D. I. Kim, “Wireless information and power transfer: rate-energy tradeoff for equi-probable arbitrary shaped discrete inputs,” *IEEE Trans. Wireless Commun.*, vol. 15, no. 6, pp. 4393–4407, Jun. 2016.
- [6] R. Zhang and C. K. Ho, “MIMO broadcasting for simultaneous wireless information and power transfer,” *IEEE Trans. Wireless Commun.*, vol. 12, no. 5, pp. 1989–2001, May 2013.
- [7] J. Park and B. Clerckx, “Joint wireless information and energy transfer in a two-user MIMO interference channel,” *IEEE Trans. Wireless Commun.*, vol. 12, no. 8, pp. 4210–4221, Aug. 2013.
- [8] K. Huang and E. G. Larsson, “Simultaneous information and power transfer for broadband downlink systems,” *IEEE Trans. Signal Process.*, vol. 61, no. 23, pp. 5972–5986, Dec. 2013.
- [9] W. Liu, X. Zhou, S. Durrani, and P. Popovski, “SWIPT with practical modulation and RF energy harvesting sensitivity,” in *Proc. IEEE Int. Conf. Commun.*, 2016, pp. 1–7.
- [10] B. Clerckx and E. Bayguzina, “Waveform design for wireless power transfer,” *IEEE Trans. Signal Process.*, vol. 64, no. 23, pp. 6313–6328, Dec. 2016.
- [11] Y. Huang and B. Clerckx, “Large-scale multiantenna multisine wireless power transfer,” *IEEE Trans. Signal Process.*, vol. 65, no. 21, pp. 5812–5827, Nov. 2017.
- [12] B. Clerckx and E. Bayguzina, “A low-complexity adaptive multisine waveform design for wireless power transfer,” *IEEE Antennas Wireless Propag. Letters*, vol. 16, pp. 2207–2210, 2017.
- [13] J. Kim, B. Clerckx, and P. D. Mitcheson, “Prototyping and experimentation of a closed-loop wireless power transmission with channel acquisition and waveform optimization,” in *Proc. IEEE Wireless Power Transfer Conf.*, 2017, pp. 1–4.
- [14] B. Clerckx, “Wireless information and power transfer: nonlinearity, waveform design and rate-energy tradeoff,” *IEEE Trans. Signal Process.*, vol. 66, no. 4, pp. 847–862, Feb. 2018.
- [15] M. Varasteh, B. Rassouli, and B. Clerckx, “Wireless information and power transfer over an AWGN channel: nonlinearity and asymmetric Gaussian signaling,” in *Proc. IEEE Inf. Theory Workshop*, 2017, pp. 181–185.
- [16] M. Varasteh, B. Rassouli, and B. Clerckx, “On capacity-achieving distributions over complex AWGN channels under nonlinear power constraints and their applications to SWIPT,” arXiv:1712.01226, 2017.
- [17] F. Killmann and E. von Collani, “A note on the convolution of the uniform and related distributions and their use in quality control,” *Economic Quality Control*, vol. 16, no. 1, pp. 17–41, 2001.
- [18] U. Madhow, *Fundamentals of Digital Communication*, New York: Cambridge University Press, 2008.
- [19] M. Chiang, “Geometric programming for communication systems,” *Found. Trends Commun. Inf. Theory*, vol. 2, pp. 1–154, 2005.
- [20] P. T. Boggs and J. W. Tolle, “Sequential Quadratic Programming,” *Acta Numerica*, vol. 4, pp. 1–51, 1995.